Title	Mode demultiplexer using angularly multiplexed volume holograms
Author(s)	Wakayama, Yuta; Okamoto, Atsushi; Kawabata, Kento; Tomita, Akihisa; Sato, Kunihiro
Citation	Optics Express, 21(10), 12920-12933 https://doi.org/10.1364/OE.21.012920
Issue Date	2013-05-20
Doc URL	http://hdl.handle.net/2115/53077
Rights	© 2013 Optical Society of America, Inc.
Type	article
File Information	oe-21-10-12920.pdf

Mode demultiplexer using angularly multiplexed volume holograms

Yuta Wakayama,[1,*] Atsushi Okamoto,[1] Kento Kawabata[1], Akihisa Tomita,[1] and Kunihiro Sato[2]

[1]*Graduate School of Information Science and Technology, Hokkaido University, Kita 14 Nishi 9, Sapporo, 064-0814, Japan*
[2]*Faculty of Engineering, Hokkai-Gakuen University, Minami 26 Nishi 11, Sapporo, 064-0926, Japan*
[*]wakayama@optnet.ist.hokudai.ac.jp

Abstract: This study proposes a volume holographic demultiplexer (VHDM) for extracting the spatial modes excited in a multimode fiber. A unique feature of the demultiplexer is that it can separate a number of multiplexed modes output from a fiber in different directions by using multi-recorded holograms without beam splitters, which results in a simple configuration as compared with that using phase plates instead of holograms. In this study, an experiment is conducted to demonstrate the basic operations for three LP mode groups to confirm the performance of the proposed VHDM and to estimate the signal-to-crosstalk noise ratio (SNR). As a result, an SNR of greater than 20 dB is obtained.

OCIS codes: (090.2890) Holographic optical elements; (060.0060) Fiber optics and optical communications; (050.7330) Volume gratings; (060.1155) All-optical networks.

References and links

1. S. Berdagué and P. Facq, "Mode division multiplexing in optical fibers," Appl. Opt. **21**(11), 1950–1955 (1982).
2. H. R. Stuart, "Dispersive multiplexing in multimode optical fiber," Science **289**(5477), 281–283 (2000).
3. A. Okamoto, K. Morita, Y. Wakayama, J. Tanaka, and K. Sato, "Mode division multiplex communication technique based on dynamic volume hologram and phase conjugation," Proc. SPIE **7716**, 771627, 771627-10 (2010).
4. Y. Kokubun and M. Koshiba, "Novel multi-core fibers for mode division multiplexing: proposal and design principle," IEICE Electron. Express **6**(8), 522–528 (2009).
5. F. Yaman, N. Bai, B. Zhu, T. Wang, and G. Li, "Long distance transmission in few-mode fibers," Opt. Express **18**(12), 13250–13257 (2010).
6. H. Kubota, H. Takara, T. Nakagawa, M. Matsui, and T. Morioka, "Intermodal group velocity dispersion of few-mode fiber," IEICE Electron. Express **7**(20), 1552–1556 (2010).
7. C. Koebele, M. Salsi, D. Sperti, P. Tran, P. Brindel, H. Mardoyan, S. Bigo, A. Boutin, F. Verluise, P. Sillard, M. Astruc, L. Provost, F. Cerou, and G. Charlet, "Two mode transmission at 2×100 Gb/s, over 40 km-long prototype few-mode fiber, using LCOS-based programmable mode multiplexer and demultiplexer," Opt. Express **19**(17), 16593–16600 (2011).
8. S. Randel, R. Ryf, A. Sierra, P. J. Winzer, A. H. Gnauck, C. A. Bolle, R.-J. Essiambre, D. W. Peckham, A. McCurdy, and R. Lingle, Jr., "6×56-Gb/s mode-division multiplexed transmission over 33-km few-mode fiber enabled by 6×6 MIMO equalization," Opt. Express **19**(17), 16697–16707 (2011).
9. H. Kubota and T. Morioka, "Few-mode optical fiber for mode-division multiplexing," Opt. Fiber Technol. **17**(5), 490–494 (2011).
10. P. Facq, P. Fournet, and J. Arnaud, "Observation of tubular modes in multimode graded-index optical fibers," Electron. Lett. **16**(17), 648–649 (1980).
11. P. Facq, F. De Fornel, and F. Jean, "Tunable single-mode excitation in multimode fibres," Electron. Lett. **20**(15), 613–614 (1984).
12. S. Shaklan, "Selective mode injection and observation for few-mode fiber optics," Appl. Opt. **30**(30), 4379–4383 (1991).
13. Y. Kawaguchi and K. Tsutsumi, "Mode multiplexing and demultiplexing devices using multimode Interference couplers," Electron. Lett. **38**(25), 1701–1702 (2002).
14. C.-P. Yu, J.-H. Liou, Y.-J. Chiu, and H. Taga, "Mode multiplexer for multimode transmission in multimode fibers," Opt. Express **19**(13), 12673–12678 (2011).
15. M. Yoshikawa and K. Kameda, "Single-mode separation for mode-division multiplexing by holographic filter," IEICE Trans. Electron. **E77-C**(9), 1526–1527 (1994).

16. T. Wakabayashi, M. Yoshizawa, and H. Kayano, "Excitation of selective multiplex mode of graded-index optical fibers by holographic filter," IEICE Trans. Electron. **E71**(2), 125–126 (1988).
17. F. Dubois, P. Emplit, and O. Hugon, "Selective mode excitation in graded-index multimode fiber by a computer-generated optical mask," Opt. Lett. **19**(7), 433–435 (1994).
18. A. Amphawan, "Holographic mode-selective launch for bandwidth enhancement in multimode fiber," Opt. Express **19**(10), 9056–9065 (2011).
19. D. Psaltis and G. W. Burr, "Holographic data storage," Computer **31**(2), 52–60 (1998).
20. K. Aoki, A. Okamoto, Y. Wakayama, A. Tomita, and S. Honma, "Selective multimode excitation using volume holographic mode multiplexer," Opt. Lett. **38**(5), 769–771 (2013).
21. E. G. Ramberg, "The hologram-properties and application," RCA Review **27**(4), 467–499 (1966).
22. K. Rastani, "Storage capacity and cross talk in angularly multiplexed holograms: two case studies," Appl. Opt. **32**(20), 3772–3778 (1993).
23. H. Kogelnik, "Coupled wave theory for thick hologram gratings," Bell Syst. Tech. J. **48**, 2909–2947 (1969).
24. J. Ikeda, R. Arai, N. Morishita, C. Katahira, Y. Takatani, S. Yumoto, K. Yokouchi, Y. Hayashi, Y. Tanaka, K. Watanabe, P. B. Lim, and M. Inoue, "Nano-gel photopolymer recording material," in *Proceedings of International Workshop on Holographic Memories and Display*, (IWHM&D, 2009), 3A–4.
25. A. Okamoto, K. Aoki, Y. Wakayama, D. Soma, and T. Oda, "Multi-Excitation of Spatial Modes using Single Spatial Light Modulator for Mode Division Multiplexing," in *Optical Fiber Communication Conference/National Fiber Optic Engineers Conference (OFC/NFOEC)*, OSA Technical Digest (Optical Society of America, 2012), paper JW2A.38.
26. A. Okamoto, K. Kunori, M. Takabayashi, A. Tomita, and K. Sato, "Holographic diversity interferometry for optical storage," Opt. Express **19**(14), 13436–13444 (2011).
27. Y. Wakayama, A. Okamoto, J. Nozawa, A. Tomita, M. Takabayashi, and K. Sato, "Two-channel algorithm for high accurate phase measurement using holographic-diversity interferometry," in *Proceedings of International Workshop on Holography and related technologies*, (IWH, 2012), Tu-I-35.
28. J. H. Povlsen, P. Danielsen, and G. Jacobsen, "Modal propagation constants, group delays, and eigenfields for practical multimode graded-index fibers," J. Opt. Soc. Am. **72**(11), 1506–1513 (1982).
29. E. Chuang and D. Psaltis, "Storage of 1000 holograms with use of a dual-wavelength method," Appl. Opt. **36**(32), 8445–8454 (1997).

1. Introduction

There has been an increase in the number of research studies on establishing a communication technology using mode division multiplexing (MDM) that is expected to improve the communication capacity per fiber by using multiple spatial modes in a multimode fiber (MMF) [1–3]. In the conventional optical communication using an MMF, a signal propagates into various spatial modes in the fiber incurring pulse broadening owing to mode dispersion. By contrast, the MDM systems distinguish the spatial modes as individual channels, and therefore, independently modulated signals in different modes are transmitted by multiplexing and are received after being separated into respective modes, without pulse broadening. Recently, high-performance fibers for MDM, such as few-mode fibers, have been studied and reported [4–9]. In addition, the technologies to excite a specific spatial mode in an optical fiber have been studied [10–14], in which mode multiplexing or demultiplexing is performed by using parallel connected and nested devices, such as phase plates and mode couplers, because, in general, each of these devices can separate only one spatial mode.

The objective of this study is to develop a device for simultaneously demultiplexing many modes without using complicated optical systems. In this paper, we propose a volume holographic demultiplexer (VHDM) configured using multi-recorded holograms that can all-optically extract specific spatial modes from the multiplexed modes including the considerably higher-order modes. The basic operations for three LP mode groups are demonstrated to confirm the performance of the proposed VHDM. In this experiment, the LP modes are produced by using computer-generated holograms (CGHs) [15–18] displayed on a spatial light modulator (SLM) and are recorded in a photopolymer by angular multiplexing. Using the CGHs, each mode field can be individually multiplexed into a hologram without distortion of the mode patterns during the MMF transmission. The signal-to-crosstalk noise ratios (SNRs) are discussed.

2. Volume holographic mode demultiplexer

The multiplexed holograms are often used as optical data storage media [19]. In comparison of the proposed demultiplexer to the data storage media, the object waves and reference waves play opposite roles in the hologram readout. In the optical data storage, the holograms are recorded as interference patterns between the object waves containing the data and the reference waves. The data contained in the object waves are reconstructed by irradiating the holograms with the reference waves used in the recording process. In the proposed demultiplexer, the holograms are multiplexed with the object waves in the specific mode fields and reference waves. The reference waves are reconstructed by inputting an MDM signal into the multiplexed holograms as the signal modes are matched with the recorded modes. The reconstructed waves are diffracted in different directions corresponding to the propagation angles of the reference waves. The VHDM, thus, works as a mode demultiplexer by using angularly multiplexed volume holograms. Moreover, it is predicted that the VHDM can operate as a multiplexer to excite the specific spatial modes in an optical fiber by functioning as an inverse demultiplexer [20].

The schematic diagram of the VHDM is shown in Fig. 1. In the recording process, writing beams W_m ($m = 1, 2, ... M$) are generated using an SLM displaying the CGHs and individually recorded while changing the incident angles of the reference beams, thus angularly multiplexing the holograms at the same spot. In the demultiplexing process, when an MDM signal S_m irradiates the multiplexed holograms, the signals in the recorded spatial modes are strongly diffracted in the directions corresponding to the reference angles set beforehand.

The diffraction properties of the VHDM can be described by referring to [21]. The m-th writing beams W_m and reference beams R_m are expressed as

$$W_m = A_m\left(x, y, z\right)\exp\left[i\phi_m\left(x, y, z\right) + ik\left(x\sin\theta_W + z\cos\theta_W\right)\right], \tag{1}$$

$$R_m = A_R\exp\left[ik\left(x\sin\theta_{Rm} + z\cos\theta_{Rm}\right)\right], \tag{2}$$

respectively, where $A_m(x, y, z)$ and A_R are the amplitudes, θ_W and θ_{Rm} are the incident angles, $\phi_m(x, y, z)$ is the phase of the mode field, k is the wavenumber defined as $k = 2\pi n_0/\lambda$, n_0 is the mean refractive index of the holographic medium, and λ is the vacuum wavelength. The use of the reference light in this study differs from the general use of volume holograms such as for optical memory. In this study, the reference light is used only during holographic writing. It is not used for irradiating the holograms during holographic reproduction. The complex amplitude transmittance T for generating the diffracted signal light is expressed as

$$T = A_R\sum_{m=1}^{M}A_m^*\left(x, y, z\right)\exp\left[-i\phi_m\left(x, y, z\right) + ikx\left(\sin\theta_{Rm} - \sin\theta_W\right) + ikz\left(\cos\theta_{Rm} - \cos\theta_W\right)\right], \tag{3}$$

where * denotes the complex conjugate.

In the mode demultiplexing process, after writing all the holograms, the time series signals $a_n(t)$ are multiplexed in different modes corresponding to the writing beams and are expressed as

$$S = \sum_{n=1}^{N}a_n\left(t\right)A_n\left(x, y, z\right)\exp\left[i\phi_n\left(x, y, z\right) + ik\left(x\sin\theta_W + z\cos\theta_W\right)\right]. \tag{4}$$

These signals are input into the multiplexed volume holograms and are diffracted as

$$D_l = \eta\int_{x=-d/2}^{x=d/2}\int_{y=-d/2}^{y=d/2}\int_{z=-L/2}^{z=L/2}TS\exp\left[-ik(x\sin\theta_{Dl} + z\cos\theta_{Dl})\right]dxdydz, \quad \left(l = 1, 2, ..., M\right) \tag{5}$$
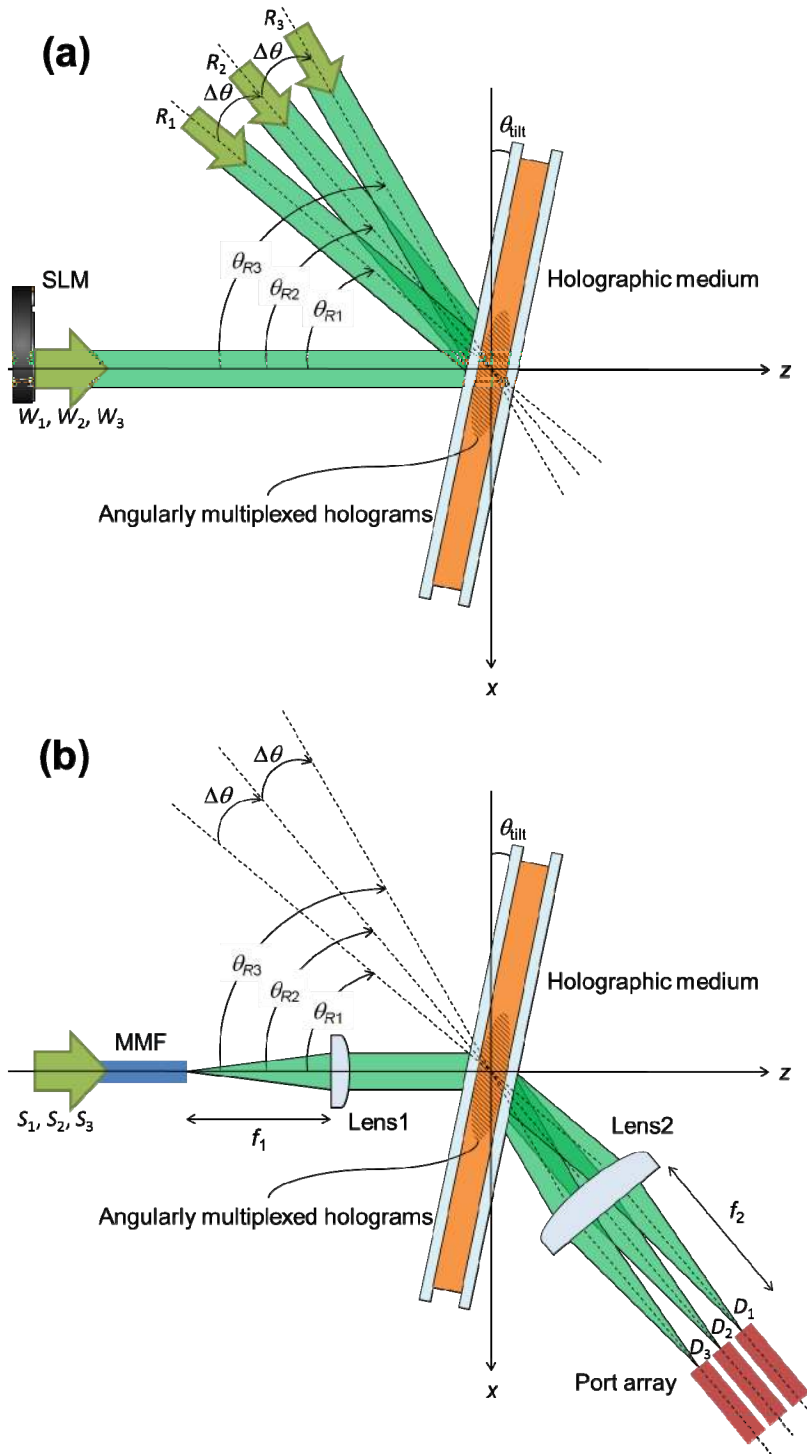
Fig. 1. Schematic diagram of volume holographic mode demultiplexer. (a) In the recording mode, writing beams W_m are incident on a holographic medium with reference beams to configure angularly multiplexed holograms. (b) In the demultiplexing mode, MDM signals S_n are extracted by irradiating the multiplexed holograms.

where d is the hologram width and L is the hologram thickness, θ_{Dl} is the diffraction direction, and η is the diffraction efficiency, that will scale as the inverse of M [22]. By substituting Eqs. (3) and (4) into Eq. (5), the following equation is derived:

$$D_l = \eta A_R \int_{x=-d/2}^{x=d/2} \int_{y=-d/2}^{y=d/2} \int_{z=-L/2}^{z=L/2}$$
$$\sum_{m=1}^{M} \sum_{n=1}^{N} a_n(t) A_m^* A_n \exp\left[i(\phi_n - \phi_m) + ikx(\sin\theta_{Rm} - \sin\theta_{Dl}) + ikz(\cos\theta_{Rm} - \cos\theta_{Dl})\right] dxdydz. \tag{6}$$

When ϕ_m and ϕ_n are matched, that is, when $m = n$, the diffracted light notably appears in the direction of $\theta_{Dl} = \theta_{Rm}$. In this case, the diffracted light is observed as

$$D_l = \eta A_R \sum_{m=0}^{M} a_m(t) \int_{x=-d/2}^{x=d/2} \int_{y=-d/2}^{y=d/2} \int_{z=-L/2}^{z=L/2} |A_m|^2 \, dxdydz. \tag{7}$$

The diffracted beams are output at different angles for each spatial mode, depending on the phase matching characteristics of the volume holograms. Thus, the MDM signal S is demultiplexed and detected with independent photodetectors at the output.

The maximum number of holograms that can be stored depends on the diffraction efficiency and angular selectivity [23]. For example, if the angular difference of the reference beam is allowed within a range of 40° and the angular selectivity is 0.5°, 80 mode signals can be demultiplexed using a single VHDM without additional optics. However, the angular shift $\Delta\theta$ shown in Fig. 1 is actually adjusted to be larger than angular selectivity because SNRs can be improved by increasing the angular shift. This also means a reduction in the number of holograms that can be written and it will be a practical limitation.

3. Experiment

A simple demonstration is performed with the experimental setup shown in Fig. 2 to confirm the basic operation of the proposed VHDM. In this experiment, three different modes are recorded on a holographic medium by angular multiplexing. In the recorded modes of the multiplexed holograms, the diffracted beams are observed by using a CCD image sensor to estimate the SNR. The mode fields of the signals are generated from the CGHs rather than from the MMF to investigate the performance of the VHDM without considerable distortion during the MMF transmission. In addition, the diffracted light signal travels in the same direction as that of the reference beam used for recording the input mode. The SNRs for the three mode groups, namely, group A (LP_{01}, LP_{11a}, and LP_{11b}), group B (LP_{11a}, LP_{11b}, and LP_{21}), and group C (LP_{01}, LP_{51}, and $LP_{10,1}$), are estimated.

A nano-gel photopolymer with a thickness of 400 μm is used as a holographic medium, which exhibits Bragg diffraction without higher-order diffracted light and shows a diffraction efficiency of 100% [24]. The tilt angle of the medium θ_{tilt} is 0° (see Fig. 1). An index modulation is induced by irradiating the polymer with green light. For this, a DPSS laser at 532 nm is used as the light source. The laser beam is cleaned up and expanded using an objective lens, a pinhole, and an achromatic lens after it serially passes through an isolator and a neutral density filter for power stabilization and attenuation, respectively. The expanded laser beam is divided into the writing and the reference arms by using a polarizing beam splitter and a half-wave plate adjusting power allocation.

In the writing arm, the mode fields are sequentially generated using an SLM displaying the CGHs, as shown in Fig. 3. The accurate generation of the mode fields is confirmed by observing the output patterns from an MMF excited with the mode fields generated by the CGHs, as reported in [20,25]. Furthermore, in this study, the phase map of the generated mode fields is observed using holographic-diversity interferometry, which is a type of advanced phase-shifting interferometry used for phase estimation [26,27]. The m-th CGH is simply calculated as an interference pattern between a mode field and a plane reference field:
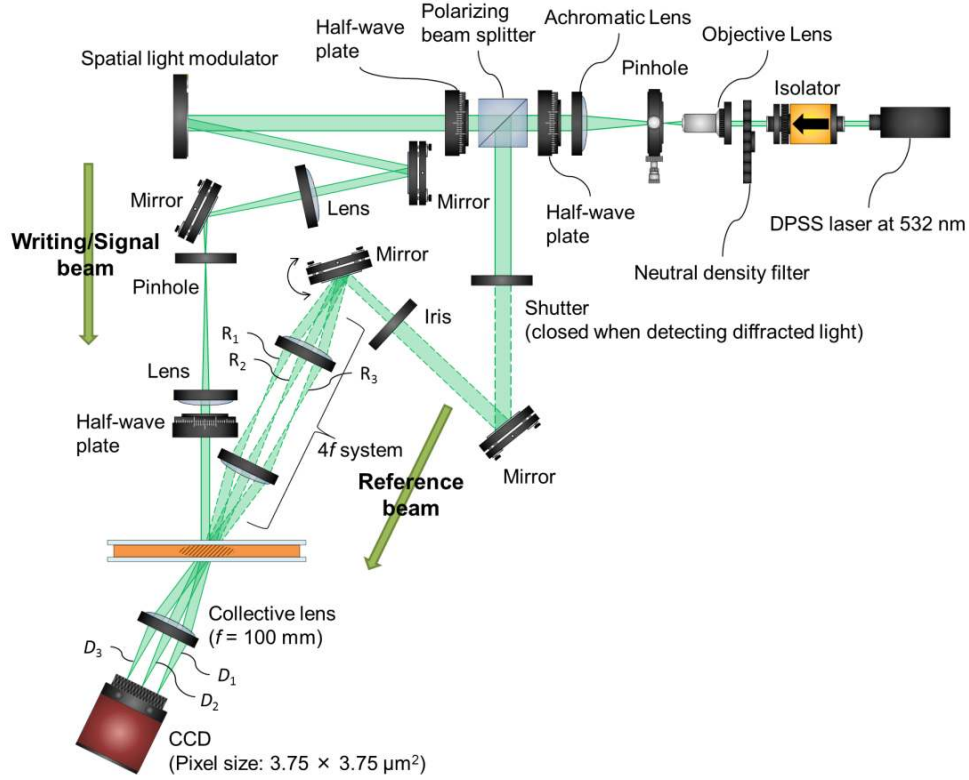
Fig. 2. Experimental setup for basic operation of proposed volume holographic mode demultiplexer and estimation of signal-to-crosstalk noise.
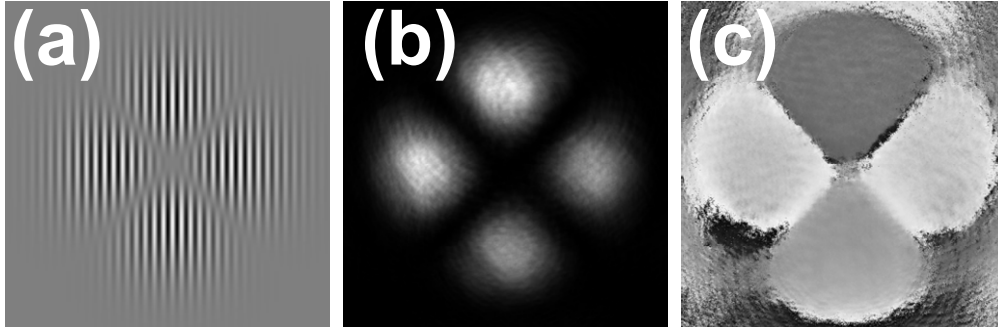

Fig. 3. Computer-generated hologram and reconstructed image. (a) CGH of LP_{21} is calculated by using Eq. (8). (b) Intensity and (c) phase of reconstructed mode field are measured using holographic-diversity interferometry (HDI).

$$\text{CGH}_m = \text{LP}_{p,q}\left(\rho, \varphi\right)\cos\left(k_0 x \theta_m\right), \qquad (8)$$

$$\text{LP}_{pq}\left(\rho, \varphi\right) = \rho^p \exp\left(-\frac{\rho^2}{2}\right) L_{q-1}^{(p)}\left(\rho^2\right)\cos\left(p\varphi\right), \qquad (9)$$

where k_0 is the vacuum wavenumber, x is the horizontal coordinate on the SLM, θ_m is the incident angle of a digital reference wave simulated using a computer, $\text{LP}_{pq}(\rho, \varphi)$ is the mode field [28] described by the spherical coordinates, ρ is the distance from the origin, φ is the argument, L is the Laguerre polynomial, and p and q are positive integers. LP_{11a} and LP_{11b} are

defined by φ of 0.5π and 0.0, respectively. The above-calculated CGHs can accurately generate the mode fields. However, it involves unnecessary higher-order diffraction because the CGH is a type of thin hologram. Therefore, a pinhole is placed after the SLM to extract the first-order diffracted light from other orders of diffracted light. The generated fields are polarized into vertically polarized light by a half-wave plate and are incident on the polymer. The beam diameters of the LP modes are adjusted by determining the size of the CGHs by assuming that a lens with a focal length of 25 mm, that is, $f_1 = 25$ mm, as shown in Fig. 1(b), is used for the collimation of the output light from a graded-index MMF with a diameter of 62.5 μm and a relative index difference of 0.01. The beam intensity is 2.7 mW/cm^2.
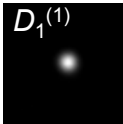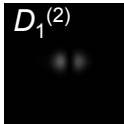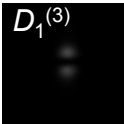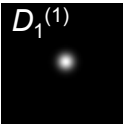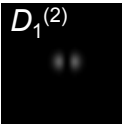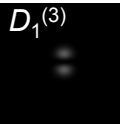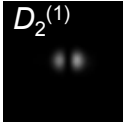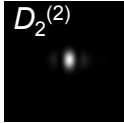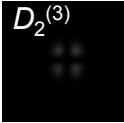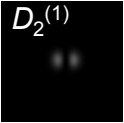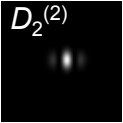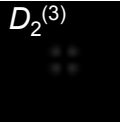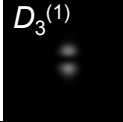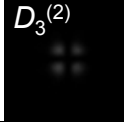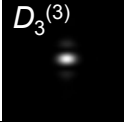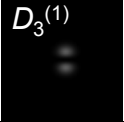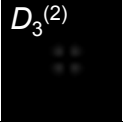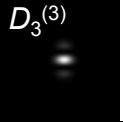
In the reference arm, the beam diameter is adjusted to 7 mm using an iris in order to make it sufficiently large compared to the diameter of the signal beam. The reference intensity is 1.3 mW/cm^2. For mode groups A and B, the incident angle of the reference beam is shifted in steps of $\Delta\theta = 1°$ using a $4f$ system between an angular variable mirror and the holographic medium. The angles θ_{R1}, θ_{R2}, and θ_{R3} are 9°, 10°, and 11°, respectively. For mode group C, θ_{R1}, θ_{R2}, and θ_{R3} are set at 20°, 30°, and 40°, respectively, such that the multiplexing angle is shifted by 10°. The angular shit is set to be sufficiently larger than the angular selectivity of 0.43° obtained by theoretical calculations [23] because crosstalk noise depends on the angular shit. In this case, the angular shift is provided by switching mirrors instead of employing the $4f$ system. This is effective for the precise extraction of a signal because the fidelity of the reference beam is higher than that of the $4f$ system with lens aberration.

In hologram recording, the polymer is irradiated for 8, 10, and 12 s for the first, second, and third holograms, respectively, to maintain the same modulation depth of the refractive index between the holograms. After recording the holograms, the reference beam is turned off for the detection of the diffracted light. The signal beams are sequentially input into the multiplexed holograms.

4. Results and discussion

This section describes the experimental and analytical results of the fundamental operations performed for three mode groups A, B, and C. Moreover, it discusses the method used for obtaining higher SNRs with the proposed VHDM.

Table 1. Images of diffracted beams for group A

Table 2. Images of diffracted beams for group B

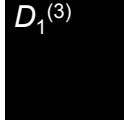|	Experiment (Group B)			Simulation (Group B)		
	1st mode LP$_{11a}$	2nd mode LP$_{11b}$	3rd mode LP$_{21}$	1st mode LP$_{11a}$	2nd mode LP$_{11b}$	3rd mode LP$_{21}$
D_1	$D_1^{(1)}$	$D_1^{(2)}$	$D_1^{(3)}$	$D_1^{(1)}$	$D_1^{(2)}$	$D_1^{(3)}$
D_2	$D_2^{(1)}$	$D_2^{(2)}$	$D_2^{(3)}$	$D_2^{(1)}$	$D_2^{(2)}$	$D_2^{(3)}$
D_3	$D_3^{(1)}$	$D_3^{(2)}$	$D_3^{(3)}$	$D_3^{(1)}$	$D_3^{(2)}$	$D_3^{(3)}$

(a)

(b)

(c)

(d)
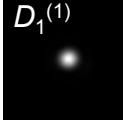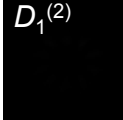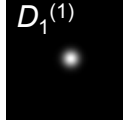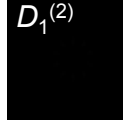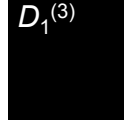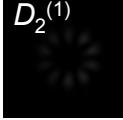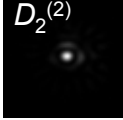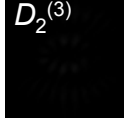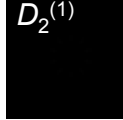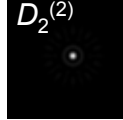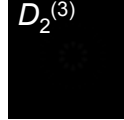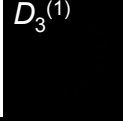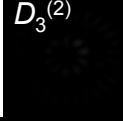
Fig. 4. Normalized power of diffracted light for mode groups A and B. The normalized values for group A are evaluated from (a) experimental and (b) numerical results. Similarly, the values for group B are calculated from (c) experimental and (d) numerical results.

Table 3. Images of diffracted beams for group C

	Experiment (Group C)			Simulation (Group C)		
	1st mode	2nd mode	3rd mode	1st mode	2nd mode	3rd mode
	LP_{01}	LP_{51}	$LP_{10,1}$	LP_{01}	LP_{51}	$LP_{10,1}$
D_1	$D_1^{(1)}$	$D_1^{(2)}$	$D_1^{(3)}$	$D_1^{(1)}$	$D_1^{(2)}$	$D_1^{(3)}$
D_2	$D_2^{(1)}$	$D_2^{(2)}$	$D_2^{(3)}$	$D_2^{(1)}$	$D_2^{(2)}$	$D_2^{(3)}$
D_3	$D_3^{(1)}$	$D_3^{(2)}$	$D_3^{(3)}$	$D_3^{(1)}$	$D_3^{(2)}$	$D_3^{(3)}$

Fig. 5. Normalized power of diffracted light for mode group C. The normalized values were evaluated from (a) experimental and (b) numerical results.
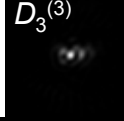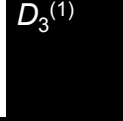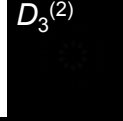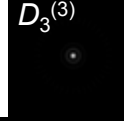
Tables 1 and 2 list the images of the diffracted beams for groups A and B, which are captured by using a CCD image sensor after focusing with a collective lens with a focal length of 100 mm. The images are trimmed into a size of 64 × 64 pixels and scaled to compare the experimental results with the theoretical data described in Section 2. The theoretical data, as listed on the right-side columns of the tables, are calculated by a computer simulation, where the size of the computational grids is defined as equivalent to the pixel size of the CCD after focusing. When an LP mode field is input into the multiplexed holograms, it is diffracted in three directions θ_{D1}, θ_{D2}, and θ_{D3} corresponding to the reference angles. The diffracted beams input in the m-th mode in all the directions are denoted as $D_l^{(m)}$, where l corresponds to the subscript number of θ_D. The diffraction efficiency η is calculated as

$$\eta = \frac{\sum_{l=1}^{3}\sum_{m=1}^{3} P_{Dl}^{(m)}}{P_{trans} + \sum_{l=1}^{3}\sum_{m=1}^{3} P_{Dl}^{(m)}}, \tag{10}$$
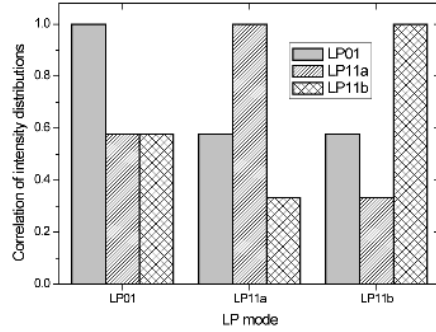
(a)
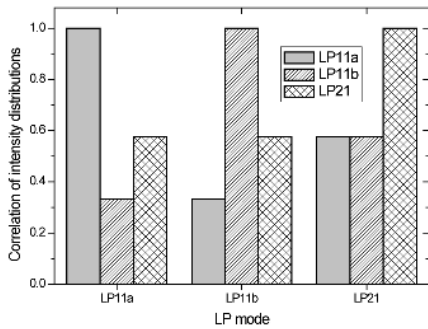
(b)
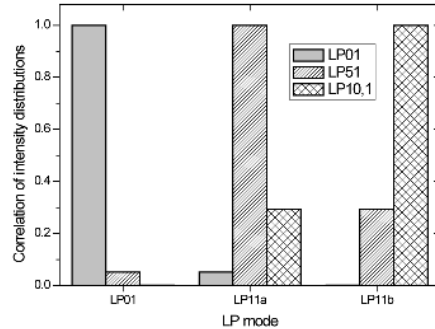
(c)

Fig. 6. Correlation of intensity distributions for LP modes of (a) group A and (b) group B. These intensity correlations are related with the normalized power of the diffracted beams shown in Figs. 4 and 5.
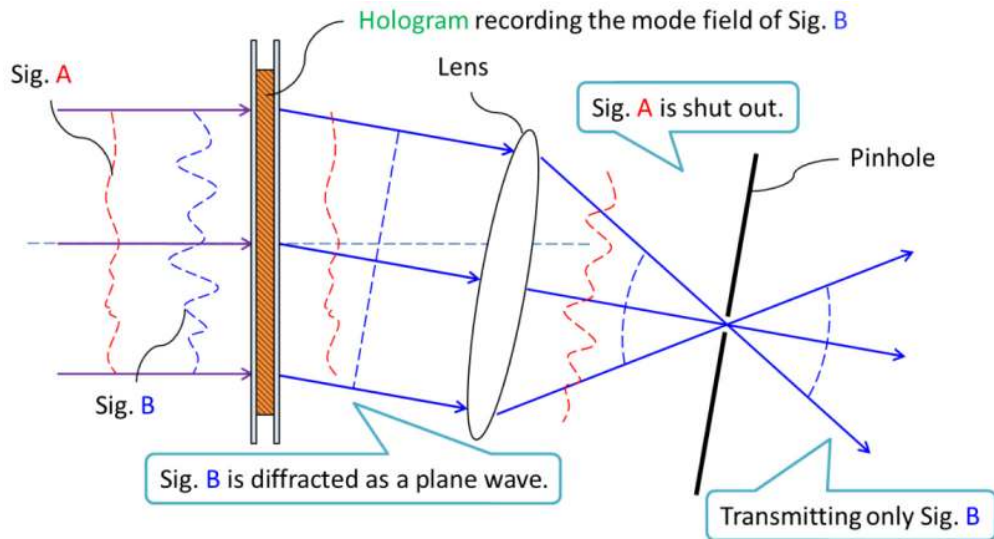
Fig. 7. Efficient mode separation using a hologram and spatial filter. A hologram recording a specific mode profile diffracts the recorded mode field as a plane wave corresponding to the wavefront of the reference beam. The diffracted plane wave can be efficiently separated by spatial filtering because it can be condensed at a single point through a lens.
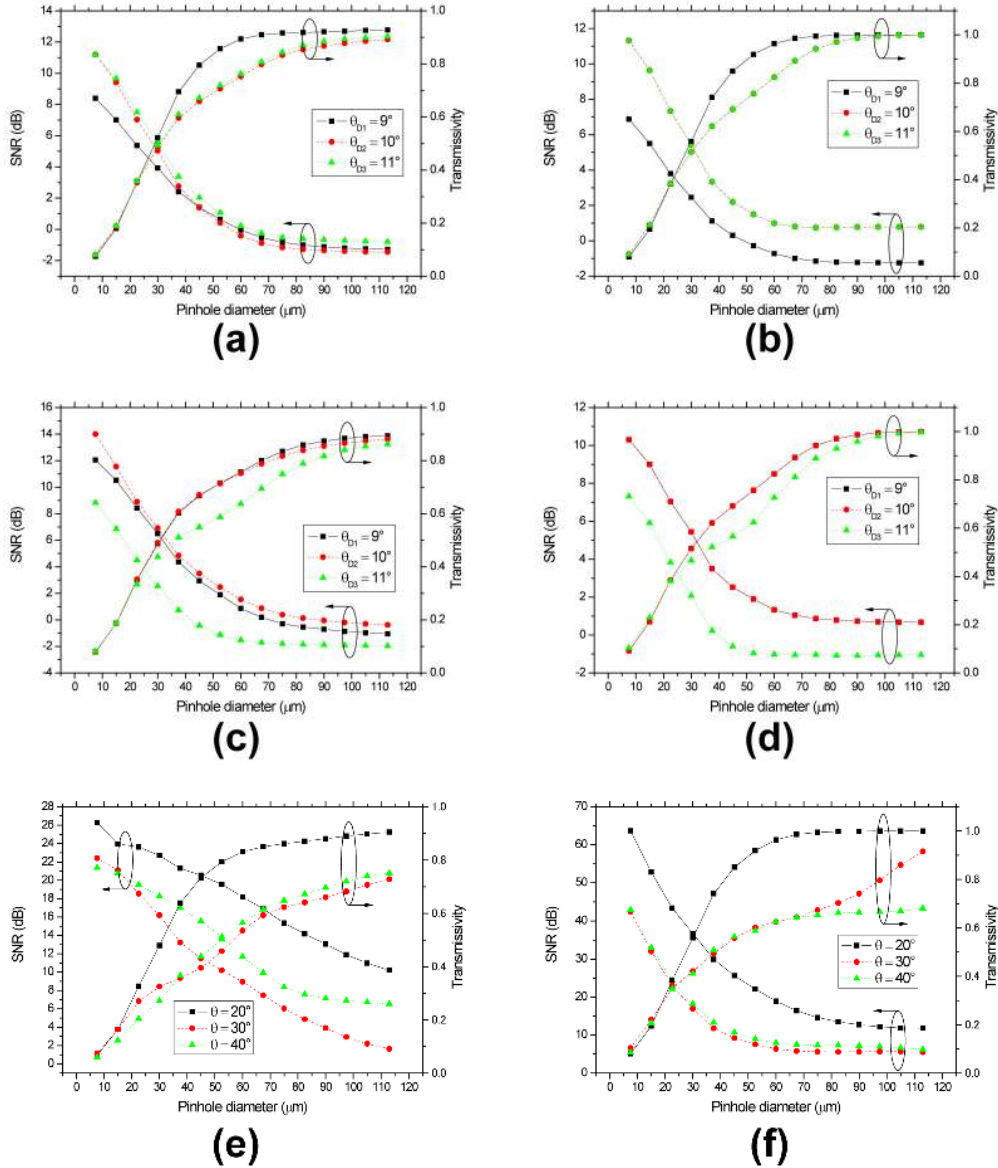
Fig. 8. SNR and transmissivity for different pinhole diameters. The graphs of (a), (c), and (e) are plotted on the basis of the experimental results for groups A, B, and C, and the graphs of (b), (d), and (f) are plotted on the basis of the numerical results for groups A, B, and C, respectively.

where $P_{Dl}^{(m)}$ is the detected power of $D_l^{(m)}$, and P_{trans} is the transmitted beam power without diffraction from the holograms. In the experimental condition, η is 72%. The transmissivity calculated as the ratio of the input and the output beam powers is 67% with reflection loss at the surface of the medium. The net efficiency calculated as the product of the diffraction efficiency and the transmissivity is 48%. In the case of LP_{01}, the input beam is strongly diffracted at θ_{D1} because LP_{01} is recorded onto the hologram at $\theta_{D1} = 9°$, whereas it is weakly diffracted at θ_{D2} and θ_{D3}. The diffracted beams are observed to comprise the combined profiles of the input mode and recorded mode. In fact, when inputting the LP_{01} into the hologram, diffracted beams $D_2^{(1)}$ and $D_3^{(1)}$ are observed to comprise the profiles of recorded modes LP_{11a} and LP_{11b}, respectively. Similarly, in the other cases, the input modes are strongly diffracted in the desired

directions, that is, $l = m$. The experimental results shown in Tables 1 and 2 are in good agreement with the numerical ones, and therefore, the fundamental operation is successfully confirmed. However, the weakly diffracted beams in the directions different from the hologram recording angle of the input mode act as crosstalk noise. Figure 4 shows the crosstalk components in all the diffraction directions. The normalized power of diffracted light $D_l^{(m)}$ is calculated as

$$\hat{P}_{Dl}^{(m)} = \frac{s_l^{(m)}}{\sum_{n=1}^{3} s_n^{(m)}} \quad (l = 1, 2, 3),$$
(11)

where $s_l^{(m)}$ and $s_n^{(m)}$ are the sums of all the pixel values of diffracted light $D_l^{(m)}$ and $D_n^{(m)}$, respectively. From these results, the SNR of D_l is estimated as

$$\mathrm{SNR}_l = \frac{\left[\hat{P}_{Dl}^{(l)} \right]^2}{\sum_{m=1}^{3} \hat{P}_{Dl}^{(m)}} \quad (l = 1, 2, 3),$$
(12)

where signal S and crosstalk noise N are defined as

$$S_l = \hat{P}_{Dl}^{(l)} \quad (l = 1, 2, 3)$$
(13)

and

$$N_l = \frac{\sum_{m=1}^{3} \hat{P}_{Dl}^{(m)}}{\hat{P}_{Dl}^{(l)}} \quad (l = 1, 2, 3),$$
(14)

respectively. The SNRs for both groups A and B never exceed 0 dB, as observed in the experiment, because of the background light in addition to the crosstalk noise.

For obtaining high SNRs, we have performed a demonstration using mode group C with a large angular shift of $\Delta\theta = 10°$ because the crosstalk noise can be suppressed by increasing the angle between the writing and the reference beams. The results for group C are obtained in a similar manner as those for groups A and B, as described in Table 3 and Fig. 5. In addition, the use of mode group C yields high SNRs because the overlapping area is extremely small in the recorded holograms owing to a low correlation of the intensity distributions in the mode fields. Thus, the crosstalk noise can be reduced using a mode group with a low intensity correlation, as shown in Fig. 6. For this reason, as shown in the results for group C, the signal components greatly outweighed the crosstalk components in contrast to those shown in the results for groups A and B.

In addition to the above theoretical prediction, the VHDM can synergistically achieve a greater SNR using a spatial filter, as shown in Fig. 7. The spatial filter aids in drawing a signal component and in blocking the noise components because the diffracted signals matching the recorded holograms comprise plane wavefronts corresponding to the reference beams and can be condensed at a single spot. As an example, Fig. 7 depicts the case where two signals A and B are input into a volume hologram storing the mode field of signal B. In this case, signal B is diffracted by the hologram as a plane wave, while signal A is diffracted as an ambiguity wave. Figures 4–6 show the diffraction characteristics in the case in which the pinhole size is sufficiently large compared to the beam diameters. On the basis of spatial filtering, the SNRs in all the diffraction directions for different pinhole diameters are evaluated by virtually setting up a pinhole by image processing, as shown in Fig. 8. The curves of LP_{11a} and LP_{11b} are equivalent because of their similar relation with LP_{01} or LP_{21}, while maintaining orthogonality. Although

the SNRs observed from the experimental results, as shown in Figs. 8(a) and 8(c), are fluctuated by the background noise, the curves obtained for small pinhole diameters are close to the theoretical results, as shown in Figs. 8(b) and 8(d), respectively. However, the experimental results shown in Fig. 8(e) differ from the theoretical results shown in Fig. 8(f). Here, the two main reasons why the theoretical and experimental results differ from each other are considered. One of the reasons is that the resolution of the actual holographic medium is limited by a large reference angle. The other reason is that there exists a difference in the optical condition between the theoretical and the experimental systems. In the actual system, mode fields are slightly spread and distorted by the optical diffraction in the free space between the SLM and the holographic medium, even when a lens system is used. In contrast, in the numerical simulation, an ideal optical system without optical diffraction is assumed. This simplification would cause a considerable difference in the SNRs when higher-order modes are used. Ideally, small beam spots are formed as observed in the theoretical results, as shown on the right-hand-side column of Table 3; obviously, the observed spots are larger than those obtained by computation, as shown on the left-hand-side column of Table 3. However, Fig. 8(e) indicates the possibility for increasing the SNRs up to 26 dB. With reference to the results, high SNRs can be achieved if a fiber array with core diameters of 10 µm is used on the focal plane instead of a CCD image sensor or a pinhole; in addition, these results indicate that the signal power is filtered out with noise abatement. In this case, although only a net signal power of 4.8% including insertion loss can pass through the 10-µm pinhole in the system assumed in this study, the results for group C show that SNRs exceeding 20 dB with a relatively higher signal power can be obtained when compared with the other groups. This observation predicts that mode selection is a key factor in determining the performance of the VHDM for different pinhole diameters.

Modal crosstalk depends on the misalignment of the optics. For example, when the center of an input mode is shifted from the center of a hologram, crosstalk increases depending on the displacement as SNR decreases. The position tolerance depends on the beam diameter and mode order of spatial modes. It decreases for higher-order modes. In the experiment, we set the diameter of the reference beam (7 mm) to be sufficiently large compared to the diameter of the writing beam (< 3 mm). Therefore, the optimum pinhole size is decided by the diameter of the writing beam rather than by that of the reference one. In contrast, when the input angle is slightly shifted from the recording angle, the SNR does not degrade notably because the balance of the signal and the crosstalk components is roughly maintained. Note that the SNR degrades substantially if the angle is critically shifted because the noise of the detection system, except for the crosstalk, cannot be ignored.

5. Conclusion

We have discussed the use of a multiplexed volume hologram for all-optical mode demultiplexing, which is regarded as a difficult problem in realizing an MDM-based communication system. The proposed VHDM can be performed with a simple setup without beam splitters; in addition, the VHDM has a unique function to extract the MDM signals on the basis of the diffraction property with angularly multiplexed holograms. In this study, the holograms are recorded and reproduced using CGHs without an MMF to confirm the demultiplexing operation and ideally estimate the SNR. The SNRs for three mode groups A, B, and C are compared. The results show that VHDM is performed along the lines of the numerical simulation without distortion during the MMF transmission. High SNRs of greater than 10 dB for all the mode groups are achieved by performing appropriate spatial filtering. Moreover, the results predict that the SNRs are inversely proportional to the intensity correlation between the mode fields. In fact, the SNRs for group C are higher than those for the other groups owing to the low intensity correlation.

The VHDM is polarization-dependent because it is based on holography. However, by utilizing a polarizing beam splitter, the proposed device can perform even if the MDM signal

shows polarization diversity. In addition, the VHDM is dependent on wavelength, based on Bragg's law. Therefore, signals at a critically different wavelength from the writing and reference beams are no longer diffracted owing to mismatch with the Bragg condition. However, the Bragg condition can be satisfied by changing the signal angle as well as the reference angle in the writing process [29]. By utilizing this characteristic, a near-infrared signal can be separated even by configuring the demultiplexer at a visible wavelength. In future work, we intend to verify this technique.